Microstructure evolution of medium-manganese Al-alloyed steel manufactured by double-step intercritical annealing

Effects of heating and cooling rates

Kozłowska, Aleksandra; Morawiec, Mateusz; Petrov, Roumen H.; Grajcar, Adam

DOI
10.1016/j.matchar.2023.112816

Publication date
2023

Document Version
Final published version

Published in
Materials Characterization

Materials Characterization 199 (2023) 112816

Contents lists available at ScienceDirect

Materials Characterization

journal homepage: www.elsevier.com/locate/matchar

Microstructure evolution of medium-manganese Al-alloyed steel manufactured by double-step intercritical annealing: Effects of heating and cooling rates

Aleksandra Kozłowska [a], Mateusz Morawiec [b], Roumen H. Petrov [c,d], Adam Grajcar [a,*]

[a] Silesian University of Technology, Faculty of Mechanical Engineering, Department of Engineering Materials and Biomaterials, Konarskiego 18a St., Gliwice 44-100, Poland
[b] Silesian University of Technology, Faculty of Mechanical Engineering, Materials Research Laboratory, Konarskiego 18a St., Gliwice 44-100, Poland
[c] Ghent University, Department of Electromechanical, Systems and Metal Engineering, Research group Materials Science and Technology, Tech Lane Ghent Science park-Campus A Zwijnaarde, Technologiepark 46, Ghent 9052, Belgium
[d] Delft University of Technology, Department of Materials Science and Engineering, 3mE-TUDelft, Building 34, Mekelweg 2, Delft 2628 CD, Netherlands

ARTICLE INFO

Keywords:
Medium-Mn steel
Multiphase microstructure
Double-step intercritical annealing
Low-C martensite
TRIP-assisted steel

ABSTRACT

A novel double-step intercritical annealing (DSIA) process was conducted on Fe-0.16C-4.7Mn-1.6Al-0.2Si transformation induced plasticity (TRIP) steel. In a present study, an effect of different heating and cooling rates applied to the second intercritical annealing (IA) step on the microstructure was studied in detail by using scanning electron microscopy (SEM), electron backscatter diffraction (EBSD) and transmission electron microscopy (TEM) techniques. The quantitative analysis of the retained austenite fractions for particular heat treatment variants was carried out via X-ray diffraction (XRD). The formation of complex microstructures containing a small fraction of ferrite, retained austenite and two types of martensite was observed regardless on the applied heating and cooling rates. It was found that the soft ferrite can be replaced by martensite through the incomplete stabilization of austenite with C and Mn during short second intercritical annealing step. The heating rate influences significantly the kinetics of austenite formation during the second heat treatment step. Low heating rates ensure more time for formation and homogenization of austenite during heating improving its thermal stability. Thus, the best balance of martensite and austenite fractions in combination with homogenous morphology of the microstructure was noted for the specimen heated at a rate of 3 °C/s, which was the lowest one in the reported experiment.

1. Introduction

Medium manganese steels containing 3–12 wt% of Mn are potential candidates suited for automotive applications, where the high strength together with good ductility are needed. Medium-Mn steels offer the product of tensile strength and total elongation at a level of 30–50 GPa% [1–3]. The beneficial mechanical properties exhibited by medium-Mn steels are attributed to the presence of metastable retained austenite (RA), which transforms into martensite upon deformation leading to transformation induced plasticity (TRIP) effect. Typically, these steels are produced via single-step intercritical annealing (IA) process in order to obtain the microstructure composed of fine ferrite (80–60 vol%) and austenite (20–40 vol%) [4–7]. The proper design of the thermal treatment schedule of IA process is crucial for obtaining an optimal balance between ferrite and austenite volume fractions of desired morphology. The IA conditions should allow for providing the effective carbon and manganese diffusion from ferrite to austenite in order to stabilize it at room temperature. The amounts of Mn and C that are partitioned into the austenite have strong influence on the effectiveness of TRIP effect and thus the final mechanical properties of steel [8,9]. Chandan et al. [5] reported that Fe-0.3C-8.1Mn-1.1Si-1.5Al steel subjected to IA showed the tensile strength of 1000–1100 MPa and total elongation at a level of 22–30%.

Besides of many advantages of intercritically annealed medium manganese steels, they show some technological problems related to the discontinuous yielding behavior [10,11] and poor local deformability of

* Corresponding author.
E-mail addresses: aleksandra.kozlowska@polsl.pl (A. Kozłowska), mateusz.morawiec@polsl.pl (M. Morawiec), roumen.petrov@UGent.be (R.H. Petrov), adam.grajcar@polsl.pl (A. Grajcar).

https://doi.org/10.1016/j.matchar.2023.112816
Received 10 January 2023; Received in revised form 26 February 2023; Accepted 10 March 2023
Available online 12 March 2023

sheet edges [12,13], which is related to the significant difference in hardness of neighboring phases leading to formation of cracks. This problem can be solved by substituting the significant part of the soft ferrite with low-carbon martensite [14–16]. Results of studies reported by Steineder et al. [17,18] and Gibbs et al. [19] show that introducing some fraction of athermal martensite can have a positive effect on the strength-ductility balance and the continuous yielding behavior of medium-Mn steels.

The novel heat treatment allowing an increase in strength and formability of medium-Mn steel sheets was first proposed by Speer et al. [14] for a 0.14C–7.17Mn–0.21Si steel. This concept assumes the application of additional intercritical annealing step before final quench. During the first IA step, which is carried out in a temperature range 650 °C–750 °C, the partitioning of C and Mn from ferrite to austenite takes place and as a result a large fraction of austenite is retained at room temperature. Afterwards, the steel is reheated to a slightly higher temperature for a short time to avoid depletion of austenite in C and Mn. The microstructure during second soaking is composed of primary austenite present after first IA step, newly formed secondary austenite and small fraction of ferrite. After final quenching to the room temperature the secondary austenite formed during second IA step transforms partially into martensite due to the low stability of this phase. The final microstructure is composed of C- and Mn-enriched primary austenite, low-C martensite and a small fraction of ferrite. So far, this type of heat treatment has not been applied for hot-rolled medium-Mn steels, in which the mechanism of austenite nucleation is different than for cold-rolled sheet steel grades [14–16,20,21].

The temperature and duration of IA heat treatment are the key parameters affecting the thermal and mechanical stability of RA. However, heating and cooling rates have also an impact on the microstructure evolution [22,23]. Jing et al. [22] reported that temperature-rise-period in a single step IA had an effect on the Mn distribution in RA grains, which significantly influence the kinetics of strain-induced martensitic transformation (SIMT). So far, this problem has not been analyzed for double-soaked medium-Mn steels. Moreover, the effects of heating and cooling rates have not been analyzed for double-soaked medium-Mn steels. Results on this issue presented in literature concern the effects of heating/cooling rates on medium-Mn steels produced via one-step IA [24–27] or first generation of TRIP steels containing 1.5–2 wt% of Mn [23]. This issue has not been analyzed for medium-Mn Al-rich steels, which is crucial for providing excellent microstructure-property balance in multiphase medium-Mn steels.

The conventional one-step intercritical annealing followed by short second IA step may improve the strength-ductility product of Al-alloyed medium-Mn steel without significant prolonging the duration of heat treatment process, what is important from the industrial point of view. The application of high heating and cooling rates during IA annealing reduces the duration of the production process. Moreover, it was reported in literature [22,28] that the application of high heating/cooling rates may also improve mechanical properties of steels with retained austenite.

Therefore, the present study addresses the influence of heating and cooling rates during the second IA step on the microstructure of Al-alloyed medium-Mn steel.

2. Material and experiments

2.1. Initial material and heat treatment

The hot-rolled 4.5 mm steel with chemical composition shown in Table 1 was investigated. To maintain weldability at an acceptable level, the chemical composition design included a carbon content of 0.16 wt%. The casting was carried out in a vacuum induction furnace using Ar protective atmosphere. Afterwards, the laboratory ingot was annealed at 1200 °C for 3 h to homogenize the distribution of alloying elements. Next, the ingot was hot-forged to the shape of 22 mm plate in a temperature range of 1200 °C–900 °C and air cooled to room temperature. Detailed information concerning the processing parameters can be found in work [29].

Table 1
Chemical composition of studied steel in wt%.

C	Mn	Al	Si	Mo	P	S	Fe
0.16	4.7	1.6	0.20	0.20	0.008	0.004	Balance

The heat treatment cycles were performed by means of dilatometry using a high-resolution BAHR dilatometer DIL805A/D. Argon was used as a cooling gas and the temperature was measured by a S-type thermocouple spot welded to the sample. Dilatometric data was analyzed in accordance with ASTM A1033–04 [30]. Specimens before heat treatment were fully austenitized and then air-quenched to the room temperature in order to provide fully martensitic microstructure. The hardenability of investigated steel is high; therefore air cooling is fast enough to obtain fully martensitic microstructure. The cylindrical specimens of 10 mm in length and 4 mm in diameter were machined from the as air-quenched material. All samples were first heated to the intercritical region at 680 °C for 30 min and then quenched at 60 °C/s to the room temperature. Results of our previous study [7] showed that the applied heat treatment conditions provide full stabilization of austenite to room temperature. After that a short secondary IA step was performed at a higher temperature (850 °C) for 30s followed by cooling to room temperature. The measured A_{c1} and A_{c3} temperatures are 648 °C and 950 °C, respectively. To characterize the effect of temperature rise/drop period on the microstructure of the investigated steel, two different heating rates were applied: slow (3 °C/s) and fast (80 °C/s) combined with two different cooling rates: slow (10 °C/s) and fast (60 °C/s). The time-temperature schedule is shown in Fig. 1.

2.2. Microstructural characterization

The microstructures were characterized by scanning electron microscopy (SEM), electron backscattered diffraction (EBSD) and transmission electron microscopy (TEM) techniques. The quantitative analysis of the fraction of RA after heat treatment was carried out via X-ray diffraction (XRD). The volume fraction of RA measured using the X-ray diffraction (XRD) method was estimated from the average of 3 measurements using the Rietveld method. XRD results were obtained using a Panalytical X'Pert Pro MPD diffractometer equipped with a cobalt source operated at an acceleration voltage of 40 kV and current of 30 mA. A step size of 0.02626° per second over the 2θ range from 40° to 115° was applied. Samples for microstructural analysis were cross-sectioned and prepared using standard metallographic procedures. They were mechanically ground with SiC paper up to 2000 grid, polished with a diamond paste (up to 1 μm) and finally with colloidal silica suspension (OPU, 35 nm); then they were etched in 4% nital solution for ~20s at room temperature (20 °C). SEM and EBSD characterizations were carried out in a FEI Quanta FEG 450. The etched samples were observed using secondary electron (SE) mode in the SEM operating at 15–20 kV accelerating voltage. The EBSD measurements were carried out on non-etched samples using a working distance of 15 mm, an accelerating voltage of 20 kV, a probe current of ~2.5 nA and a sample tilt of 70°. Hexagonal scan grid scans were performed over an area of 16 × 16 μm^2 with a step size of 0.025 μm. The orientation data were postprocessed with OIM-TSL® data Analysis software v. 7.3.1 after applying one step grain confidence index (CI) standardization clean up procedure. The remained pixels with a confidence index CI < 0.1 were removed from the collected EBSD data. Transmission electron microscope (TEM) Titan 80–300, FEI S/TEM equipped with high angular annular dark field (HAADF) and bright field/dark field (BF/DF) detectors and energy-dispersive X-ray spectroscopic (EDS) apparatus operating at an accelerating voltage 300 kV was used to reveal microstructural details.

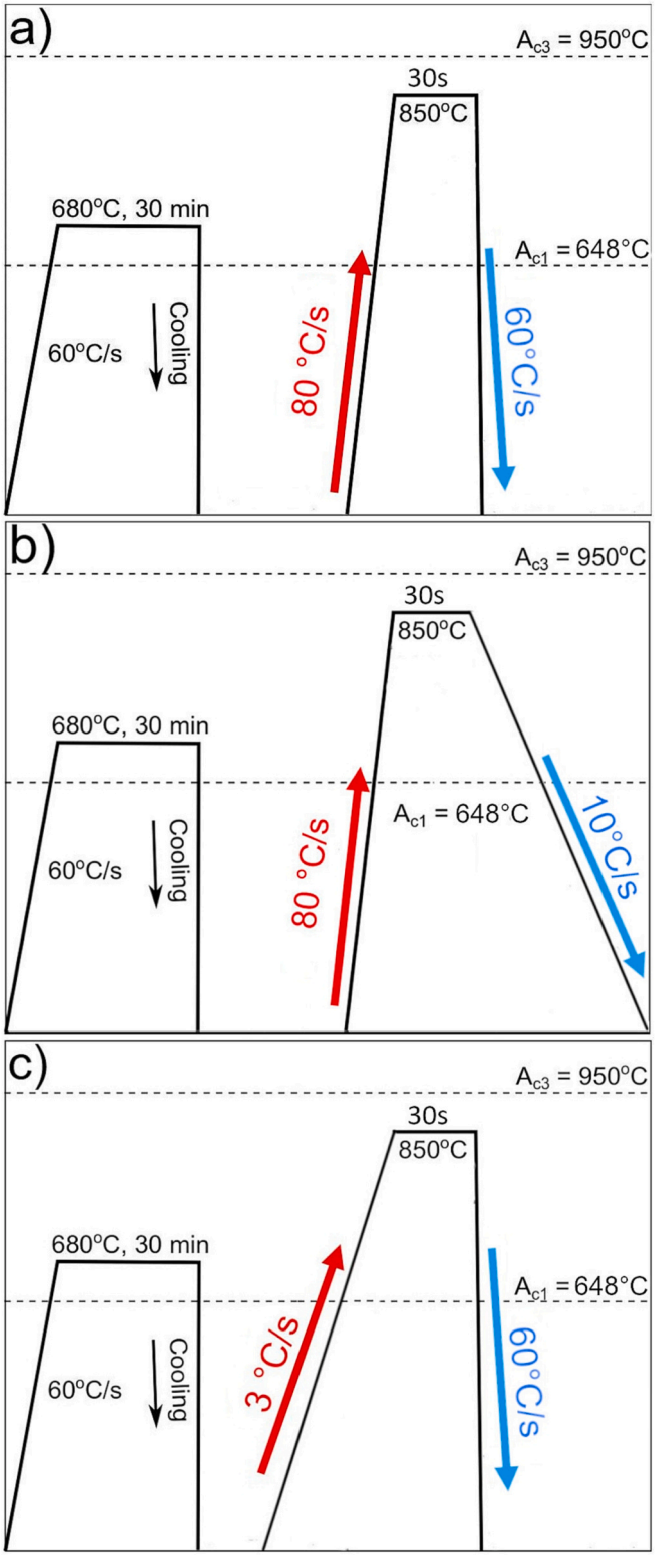

Fig. 1. The time-temperature schedules for investigated specimens. Second intercritical annealing at 850 °C, heated (red arrow) and cooled (blue arrow) at rates of: a) 80 °C/s and 60 °C/s, b) 80 °C/s and 10 °C/s, c) 3 °C/s and 60 °C/s, respectively. (For interpretation of the references to colour in this figure legend, the reader is referred to the web version of this article).

3. Results and discussion

3.1. Dilatometric results

Before the second IA step, the microstructure of samples was composed of ferrite, lath-type austenite and some fraction of martensite. Phase transformations during the second IA step were monitored using dilatometry. During the second IA step at 850 °C for 30 s, the transformation of ferrite to secondary austenite is evident through a reduction in a sample length (Fig. 2). On the basis of the results presented in Fig. 2 and Fig. 3, it can be seen that the heating rate has a significant effect on the kinetics of austenite formation during annealing. In case of slow heating (3 °C/s), the nucleation rate of austenite was significantly smaller (Fig. 3) than during heating at a rate of 80 °C/s. Austenite already begins to form gradually during heating because the process time is much longer, which allows diffusion to take place. Then, during holding this transformation continues. Comparing the dilatometric curves during the soaking time, it can be seen that after heating at a rate of 80 °C/s, the nucleation of austenite begins immediately after reaching the annealing temperature. The fraction of austenite formed in specimen heated at a higher rate is higher, when compared to the specimen heated at a rate of 3 °C/s. However, the retained austenite is not chemically homogenous due to short duration of the heating process and thus its thermal stability is reduced.

Upon quenching to the room temperature from the second IA step, an increase in a sample length characteristic for the fresh martensite formation was noted for all samples (Fig. 4). The investigated steel, regardless of the applied heating/cooling conditions, showed quite different thermal stability of RA. A slightly higher fraction of fresh martensite was formed in the specimen heated and cooled at the highest rates: 80 °C/s and 60 °C/s, respectively. The measured M_s temperature was the highest in this case: 260 °C and as a result, the highest fraction of fresh martensite was formed during cooling to the room temperature. The low stability of RA can be related to the shorter diffusion distance of Mn due to the short heating time. A higher heating rate may result in local manganese and carbon heterogeneities due to the short time for homogenization of the newly formed austenite [23]. For the slow heating rate (3 °C/s), there is more time for diffusion related to the C/Mn enrichment of RA. For the slowest heating rate (3 °C/s), the material is heat treated for 91 s until cooling begins. This time consists of the heating from the temperature of 668 °C to 850 °C (it takes 61 s) and isothermal holding at 850°s (30 s). At the high heating rate (80 °C/s), the total duration of heating from 668 °C to 850 °C drops from 61 s to about 2 s. The dissolution kinetics of Mn-rich cementite is much slower than

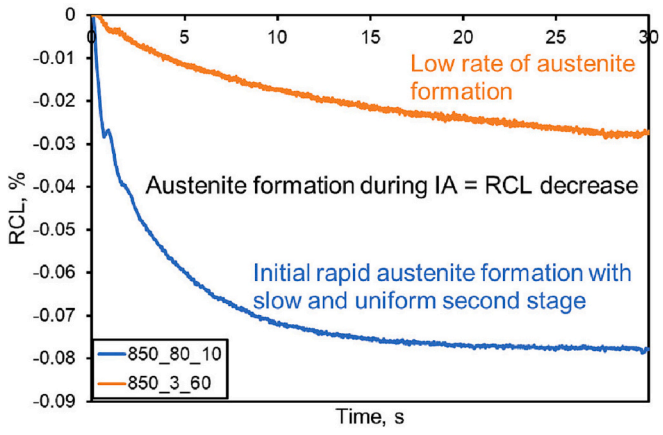

Fig. 2. The dilatometric curves during soaking at the second step of intercritical annealing at 850 °C. Specimens heated and cooled at rates of: 80 °C/s and 10 °C/s (blue), 3 °C/s and 60 °C/s (orange), respectively. (For interpretation of the references to colour in this figure legend, the reader is referred to the web version of this article).

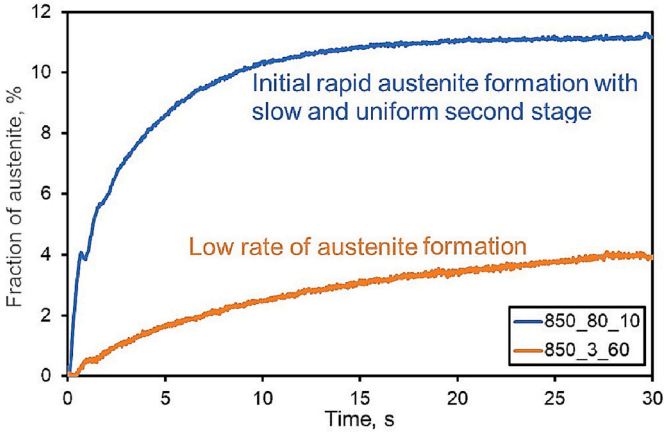

Fig. 3. The kinetics of austenite formation during the second step of intercritical annealing at 850 °C. Specimens heated and cooled at rates of: 80 °C/s and 10 °C/s (blue), 3 °C/s and 60 °C/s (orange), respectively. (For interpretation of the references to colour in this figure legend, the reader is referred to the web version of this article).

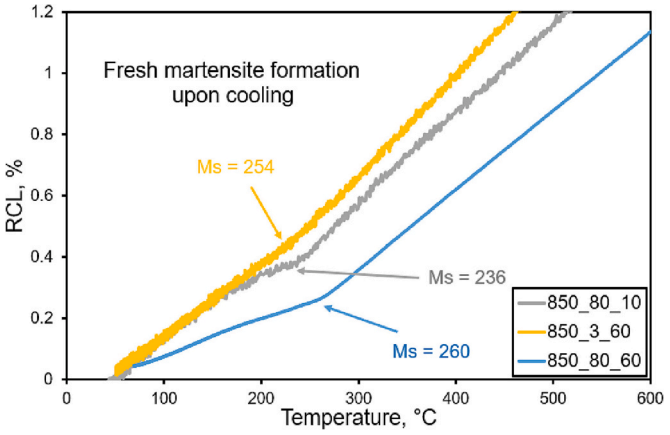

Fig. 4. The dilatometric curves registered during cooling at various rates after second step of intercritical annealing at 850 °C; M_s = 260 °C (blue); M_s = 254 °C (yellow); M_s = 236 °C (grey). (For interpretation of the references to colour in this figure legend, the reader is referred to the web version of this article).

for cementite containing only Fe and C [31]. At the highest heating rate 80 °C/s the dissolution of Mn trapped in Mn-rich cementite was limited and thus the stability of RA in this specimen was the lowest. The higher heating rate used in these samples reduces the time for enriching the austenite in carbon and manganese [22]. This reduction is so significant that it cannot be compensated by the soaking time of 30s. Therefore, RA characterized by reduced stability can be present in the microstructure. Moreover, the application of a high cooling rate favors martensitic transformation. Han et al. [32] reported that the gradient of Mn content in primary austenite gradually decreased with increasing annealing time.

3.2. *Microstructure characterization*

The microstructure after first IA step was composed of ferrite, lath-type austenite and some fraction of martensite as shown in Fig. 5a. Numerous fine carbide precipitates are located inside the martensitic laths (Fig. 5b). Such microstructure is typical for austenite reverse transformation (ART) process [31,33]. Mueller et al. [31] observed the presence of Mn-enriched cementite during IA, which was dissolving very slowly and thus some fraction of carbides stayed stable at the room temperature.

The presence of cementite in the specimen after fist IA step was confirmed by TEM analysis. (Fig. 6). Mn-rich cementite is commonly present in the microstructure of medium-Mn steels after the first IA step [31]. Some potential equilibrium fraction of M_7C_3 carbides is predicted based on the thermodynamic calculations (Fig. 7). However, their fraction is a few times lower compared to the cementite fraction, which is dominant. The applied non-equilibrium cooling rate decreases the opportunity for M_7C_3 precipitation. Therefore, the M_7C_3 carbides were not identified and observed in TEM studies.

The goal of the second IA step at a higher temperature is to replace partially or completely the ferrite with austenite during heating and soaking [14]. During final cooling some fraction of new-formed austenite transforms into fresh martensite, thus replacing the ferrite + austenite microstructure with a microstructure containing martensite, austenite and small fraction of ferrite [15]. The mechanism of austenite enrichment in C and Mn during second IA step is different than for the first IA step. It is well documented in literature [31] that Mn-rich carbides are formed during first IA step, which is typically conduced in a temperature range 650–700 °C. Formation of such carbides affects the amount and stability of retained austenite (RA) because lower concentrations of C and Mn are available in the solid solution. In the present study, all fraction of cementite dissolved during second IA because the second IA was conducted at a higher temperature (850 °C), at which Mn-rich cementite is not present according to Thermo-Calc calculations (Fig. 7). It is beneficial because carbon and manganese were released

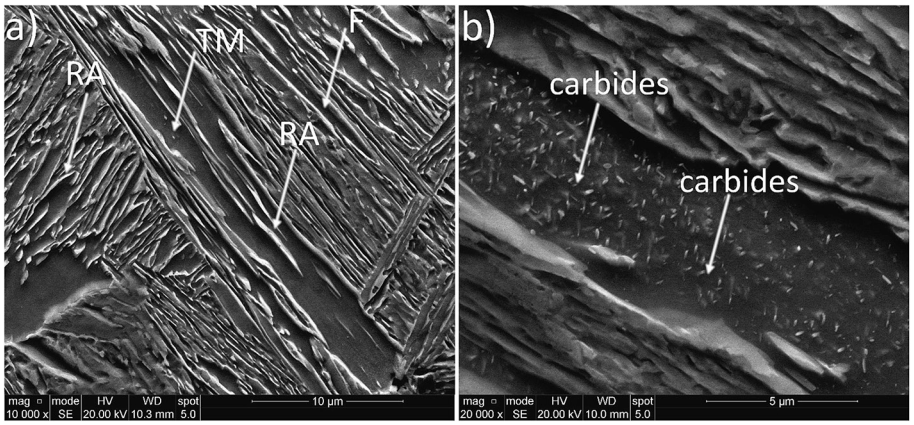

Fig. 5. Microstructure of investigated steel after the first IA step performed at 680 °C for 30 min (a); carbides formed inside tempered martensite laths after the first IA step performed at 680 °C (b). F – ferrite, RA – retained austenite, TM – tempered martensite.

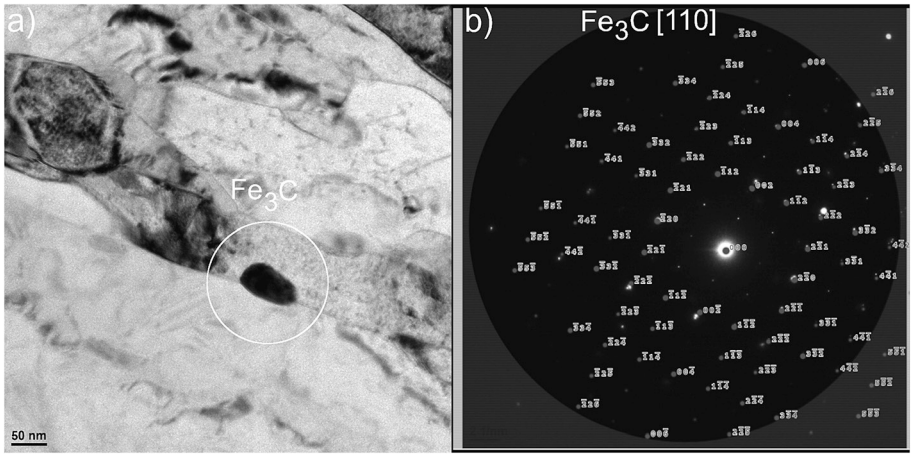

Fig. 6. TEM image of the specimen after first IA step: a) TEM bright field - cementite marked in the white circle, b) selected area electron diffraction pattern of cementite.

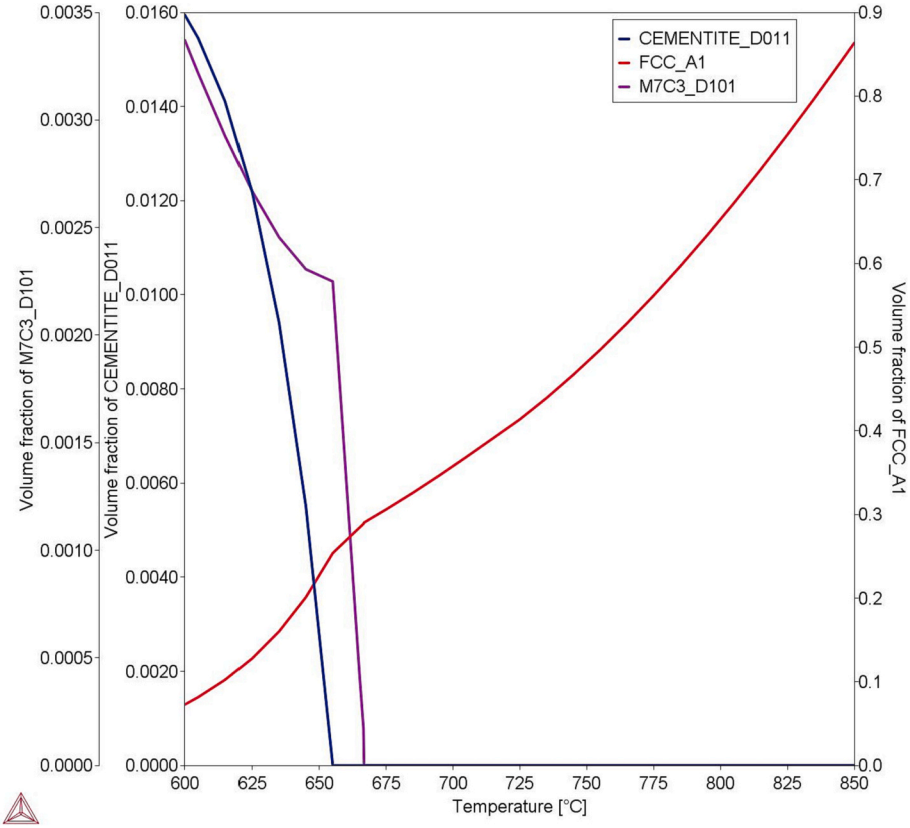

Fig. 7. Change in the fractions of austenite, cementite and M_7C_3 carbides in the annealing temperature range from 600 °C to 850 °C.

from the carbides and enriched the austenite. The applied heating rate affects the intensity of dissolution of Mn-rich carbides and thus RA of different stability was present in the microstructure.

The micrographs of specimens after second step of IA at 850 °C are shown in Fig. 8. The microstructure after second step of IA contains martensite, fine-dispersed RA and small fraction of ferrite. Two types of martensite can be observed in the microstructure. Martensite laths (M1) and small blocky non-etched martensite regions (M2) – Fig. 8a-c.

Such dual-type martensite morphology can be related to the differences in a carbon and manganese content in austenite. The austenite which is less enriched in C/Mn can transform into martensite earlier (a higher M_s temperature) during final cooling; thus this type of martensite is better developed and the substructure is visible. The non-etched martensite probably was formed later at a lower M_s temperature as a result of transformation of primary austenite present in the microstructure before second IA or austenite that was more enriched in C/Mn during second IA step [34]. The microstructure of the specimen heat-treated by using the highest heating and cooling rates seems to be more heterogeneous (Fig. 8a). It is due to the shorter time for homogenization of C/Mn distribution in the individual austenite grains. Due to short duration of second IA step (30s), the full homogenization of newly formed austenite in terms of C and Mn contents was not possible because Mn slows the dissolution rate of C in cementite. The C/Mn content in RA formed at ferrite-cementite interface is higher than in RA formed at

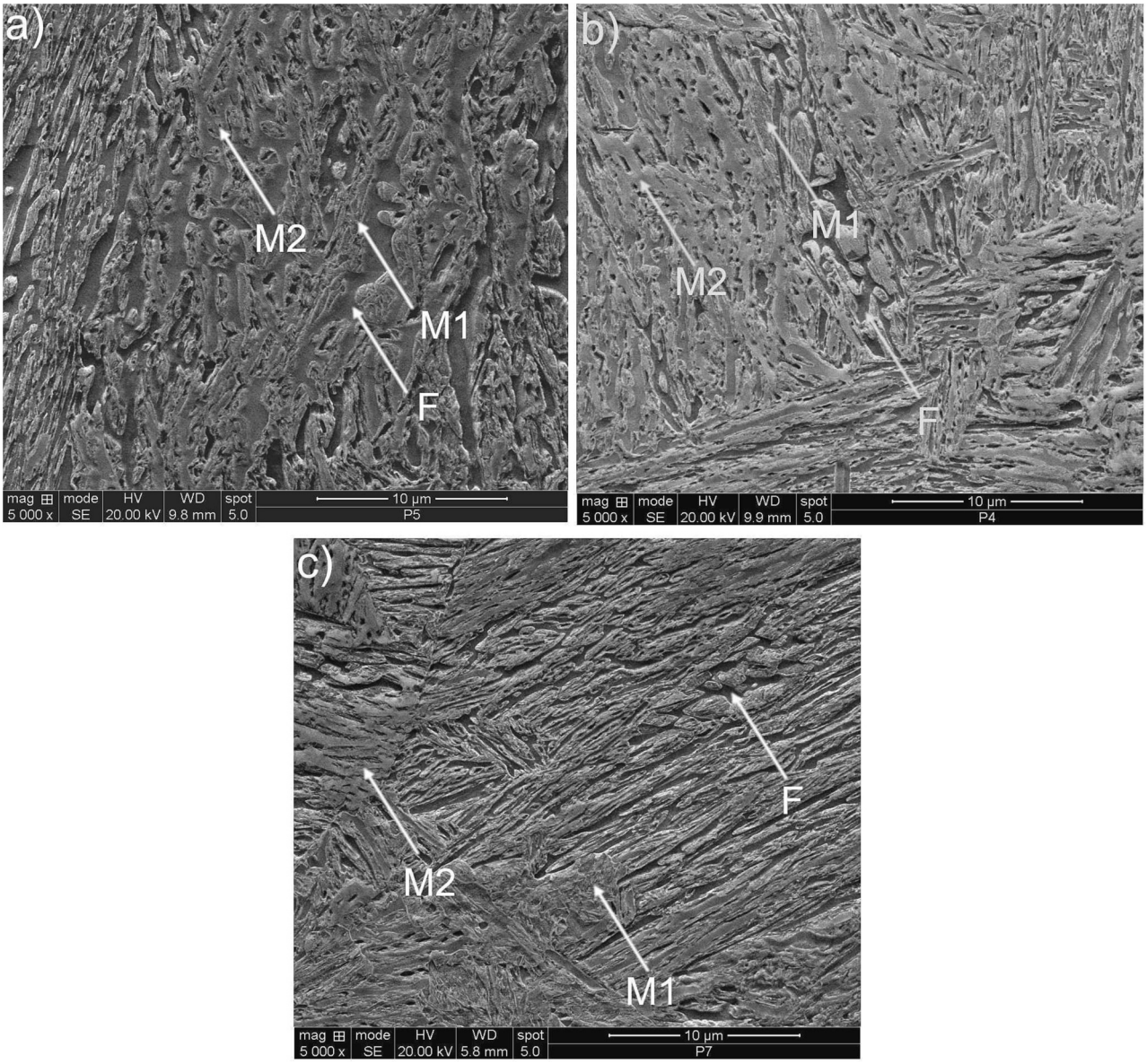

Fig. 8. Microstructure of the steel after second IA step performed at 850 °C for 30s, heated and cooled at rates of: a) 80 °C/s and 60 °C/s, b) 80 °C/s and 10 °C/s, c) 3 °C/s and 60 °C/s; F – ferrite; M1 – martensite formed earlier during final cooling; M2 – martensite formed later during final cooling to the room temperature.

ferrite grain boundaries [31]. Therefore, it is logical to assume that a RA characterized by different stability is present in the microstructure (Fig. 8a-c).

The methodology for distinguishing M1 and M2 martensites is based on the approach used for quenching and partitioning steels [35]. In this type of steels some fraction of martensite (called M1 martensite) forms during quenching (first step of QP-type heat treatment) besides of austenite. During second step (partitioning) austenite is stabilized by carbon partitioning from martensite laths. However, some fraction of unstable austenite transforms into martensite upon final cooling to room temperature. This type of martensite (called M2-martensite) is characterized by high dislocation density due to its relatively low M_s temperature. Figs. 9a, 10a and 11a show the image quality (IQ) maps combined with phase distribution maps. RA (marked in blue) in a form of thin layers or very fine grains located between the martensite laths or ferrite was observed in all samples. However, the highest fraction of this phase was noted for the specimen heated with the lowest rate (Fig. 9a). RA of film-type morphology is more stable than RA in a form of large blocky grains due to its higher carbon content. A lattice distorted by crystalline defects, such as dislocations, subgrain boundaries, and internal stresses affected a Kikuchi pattern quality leading to lower IQ values [36,37]. Dislocations and stacking faults present in a blocky-type austenite are the zones of martensite nucleation [37]. EBSD maps indicate that the differences in applied heating and cooling rates have no substantial effect on the size and morphology of RA. The differences in the heating rates were not sufficient to cause the grain refinement effect [23]. The results of STEM observations presented in Fig. 12 show that the applied heating/cooling rate ranges have no significant effect on the grain size and morphology of all microstructural constituents. The thickness of martensite laths is in a range from ~50 nm to ~300 nm independently on the applied heating/cooling rate.

EBSD maps (Fig. 9b, 10b, and 11b) show that ferrite observed on IQ maps is located in the brightest areas with the highest pattern quality due to the lowest dislocation density. In the present study, the M1 and M2 types of martensite are characterized by different C/Mn content and also different defects density. Martensite with a low C/Mn content (M1), which was formed as a result of transformation of C/Mn-depleted austenite during final cooling, can be also observed in the areas of

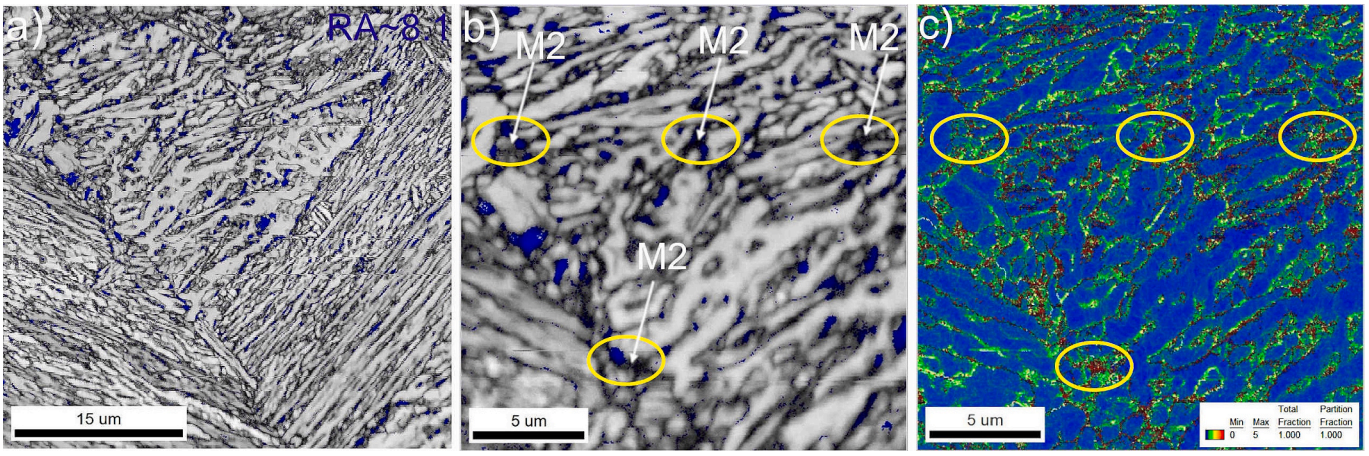

Fig. 9. EBSD maps of investigated steel after second IA step performed at 850 °C for 30s, heated and cooled at rates of 3 °C/s and 60 °C/s, respectively: a) and b) image quality maps (different magnifications) combined with phase distribution map (RA marked in blue); c) kernel average misorientation (KAM) map; M2 – martensite formed later during final cooling to the room martensite (yellow circles). (For interpretation of the references to colour in this figure legend, the reader is referred to the web version of this article).

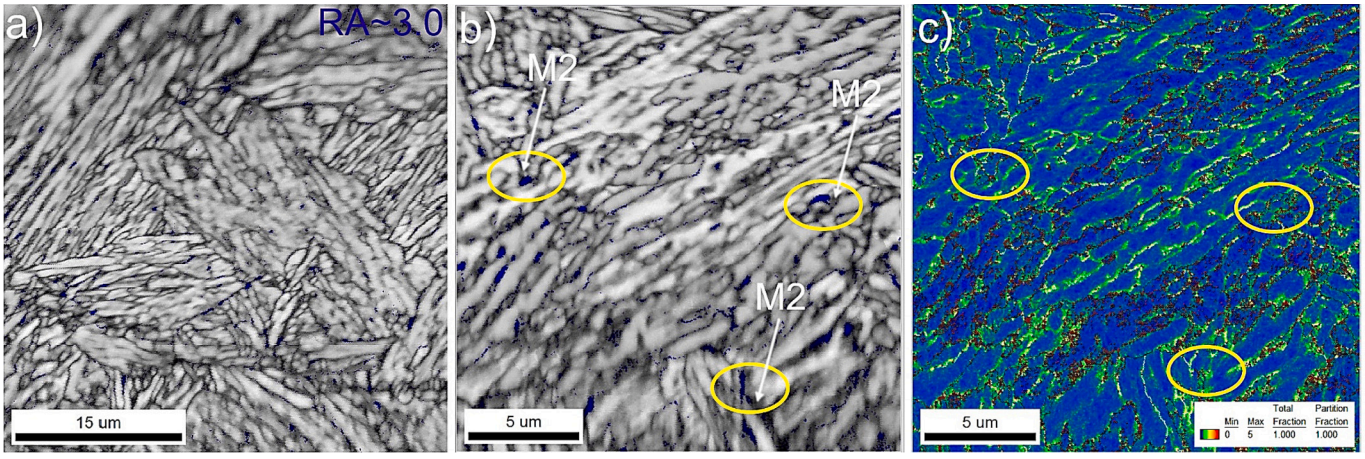

Fig. 10. EBSD maps of investigated steel after second IA step performed at 850 °C for 30s, heated and cooled at rates of 80 °C/s and 10 °C/s, respectively: a) and b) image quality maps (different magnifications) combined with phase distribution map (RA marked in blue); c) kernel average misorientation (KAM) map. M2 – martensite formed later during final cooling to the room martensite (yellow circles). (For interpretation of the references to colour in this figure legend, the reader is referred to the web version of this article).

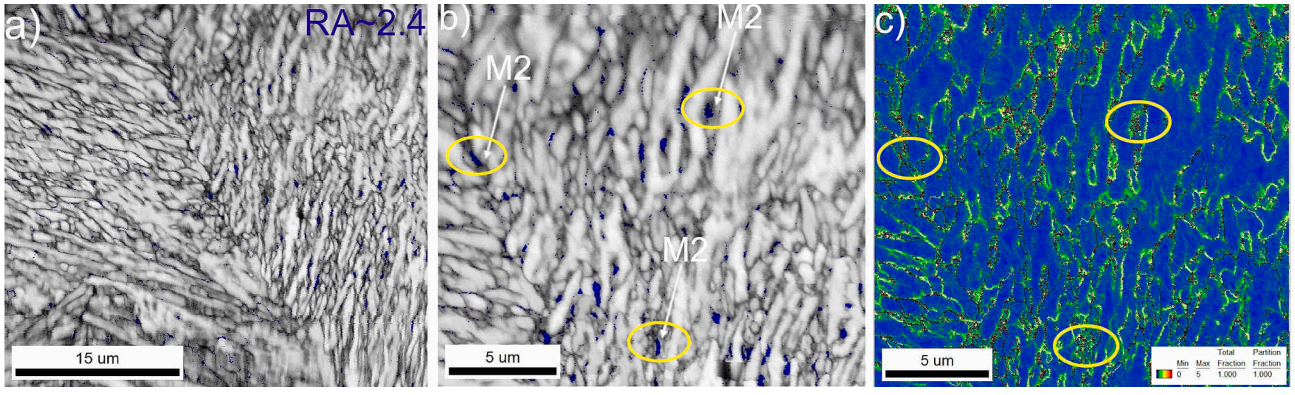

Fig. 11. EBSD maps of investigated steel after second IA step performed at 850 °C for 30s, heated and cooled at rates of 80 °C/s and 60 °C/s, respectively: a) and b) image quality maps (different magnifications) combined with phase distribution map (RA marked in blue); c) kernel average misorientation (KAM) map; M2 – martensite formed later during final cooling to the room martensite (yellow circles). (For interpretation of the references to colour in this figure legend, the reader is referred to the web version of this article).

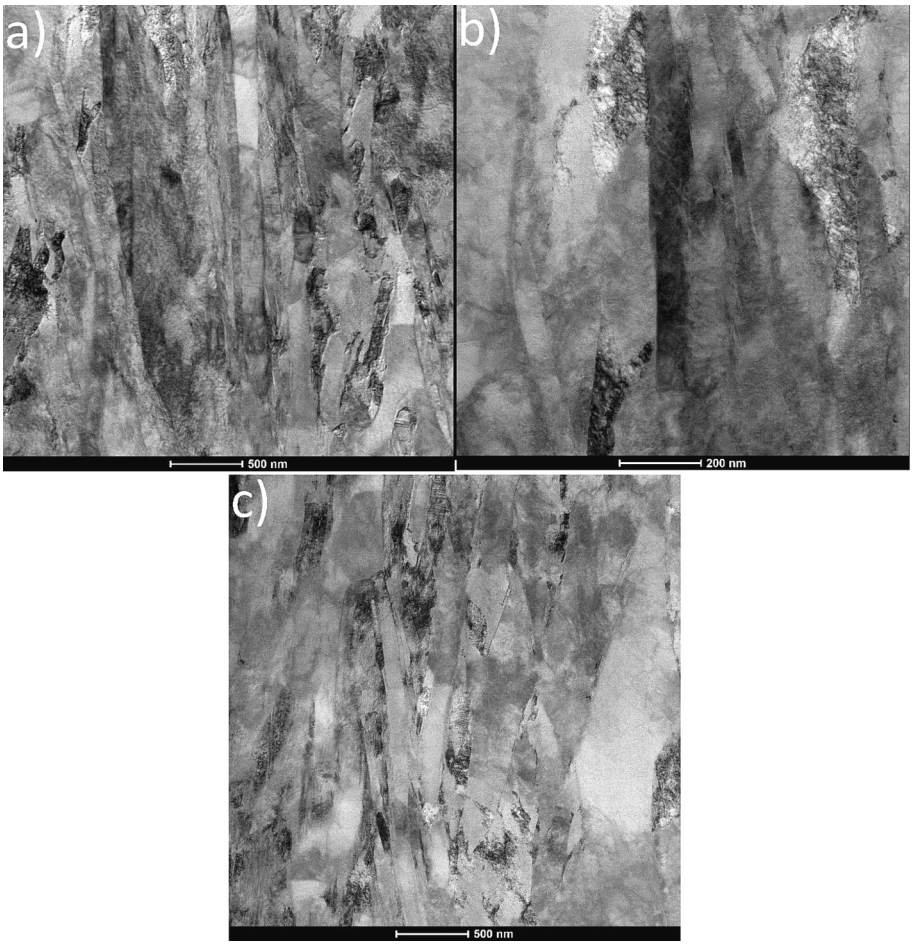

Fig. 12. STEM images of the specimen heated and cooled at rates of: a) 80 °C/s and 60 °C/s, b) 80 °C/s and 10 °C/s, c) 3 °C/s and 60 °C/s; in all cases laths' thickness range is from 50 to 300 nm.

high IQ parameter due to less density of dislocations. This martensite has also a higher M_s temperature. Martensite (M2) formed during final cooling as a result of transformation of austenite with a higher C/Mn content represents the areas with the lowest IQ parameter due to higher lattice distortions (Fig. 9b, 10b, 11b). The retained austenite is located in darker areas of intermediate IQ value. The high-C and high-Mn martensite has low M_s temperature. In order to more precisely indicate areas of different dislocation density, kernel maps were also analyzed (Fig. 9c, 10c and 11c).

The areas represented by martensite with higher C/Mn content (M2) were marked on kernel maps (Fig. 9c, 10c and 11c). They were also identified using linear analysis of IQ parameter (Fig. 13) whereas Fig. 14 shows the selected areas with the lowest IQ parameter corresponding to the M2-type martensite. The linear analysis of IQ parameter distribution in the specimen after second IA step heated at rate of 3 °C/s and cooled at 60 °C/s (Fig. 13) shows that RA is located near martensite with a higher C/Mn content (M2). This type of martensite is characterized by higher hardness than the low-C martensite (M1). Hence, the RA is stabilized through hydrostatic pressure provided by this microstructural constituent [38]. However, the presence of M2-type martensite in the microstructure may have a negative effect on mechanical properties because hard regions can act as stress concentrators and potential crack initiation sites. Such tendency was observed by Diego-Calderon et al. [39] and De Knijf et al. [35] in Quenching and Partitioning (QP) steels. They found that fresh martensite with high dislocation density triggered the void formation. It is related to its lower ductility and lower ability to accommodate the deformation. The interfaces between M2 martensite and M1 martensite or M2 martensite and RA may act as potential nucleation sites for voids and/or cracks. The regions containing microstructural constituents characterized by very low IQ parameter were highlighted in Fig. 14b. Such regions correspond to M2-type martensite (Fig. 14c). It can be seen that such areas are not dominant in the microstructure, which is advantageous in terms of mechanical properties [35,39].

The TEM (transmission electron microscopy) and STEM (scanning transmission electron microscopy) techniques allowed to distinguish the individual structural constituents (Fig. 15). The RA nucleated at grain boundaries of ferrite was less enriched in Mn (~7.1–8.2 wt%, point 1), while the RA formed at ferrite-cementite interfaces was more enriched (~11.4 wt% Mn, point 2) – Fig. 15a and b. It is also documented in literature [40] that for the short intercritical annealing at 650 °C within 3–35 s, a small increase of Mn content in austenite was observed besides of RA enrichment in C. The differences of Mn content in austenite affects its stability. TEM bright field image and selected area electron diffraction (SAED) pattern corresponding to the retained austenite obtained for the specimen heated and cooled at rates of 80 °C/s and 60 °C/s were shown in Fig. 15c and Fig. 15d, respectively. The presence of thin RA laths with a thickness of 50 nm was observed.

The results obtained by using EBSD technique refer to relatively small areas of the specimen; thus quantitative analysis of the RA fraction is not very accurate [41]. Therefore, the X-ray diffraction method was used to evaluate better statistically the volume fraction of RA obtained for different heat treatment conditions (Table 2). The volume fraction of retained austenite in the initial state (after first IA) was calculated as 19.4%. The microstructure after second IA step contains martensite, fine-dispersed RA and small fraction of ferrite. During annealing at

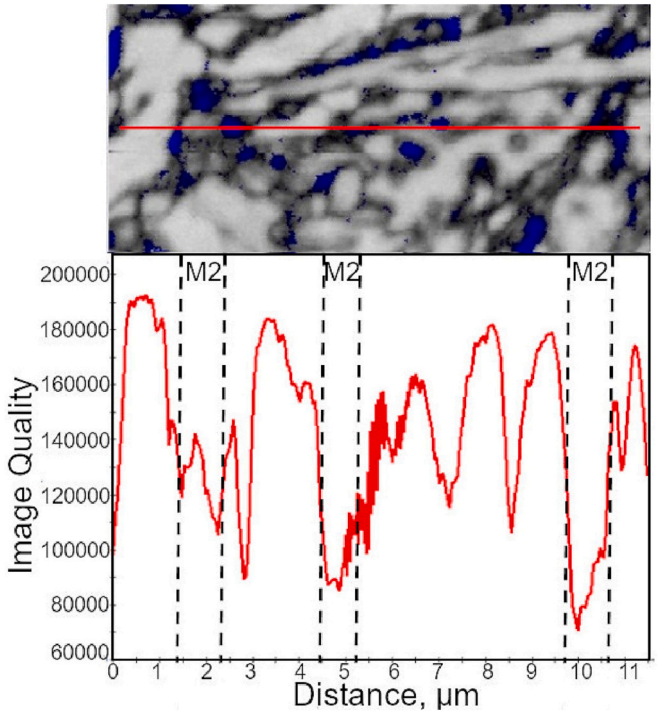

Fig. 13. Image quality map combined with phase distribution map (RA marked in blue) and linear analysis of IQ parameter after second IA step performed at 850 °C for 30s, heated and cooled at rates of 3 °C/s and 60 °C/s, respectively, M2 – martensite formed later during final cooling to the room temperature. (For interpretation of the references to colour in this figure legend, the reader is referred to the web version of this article).

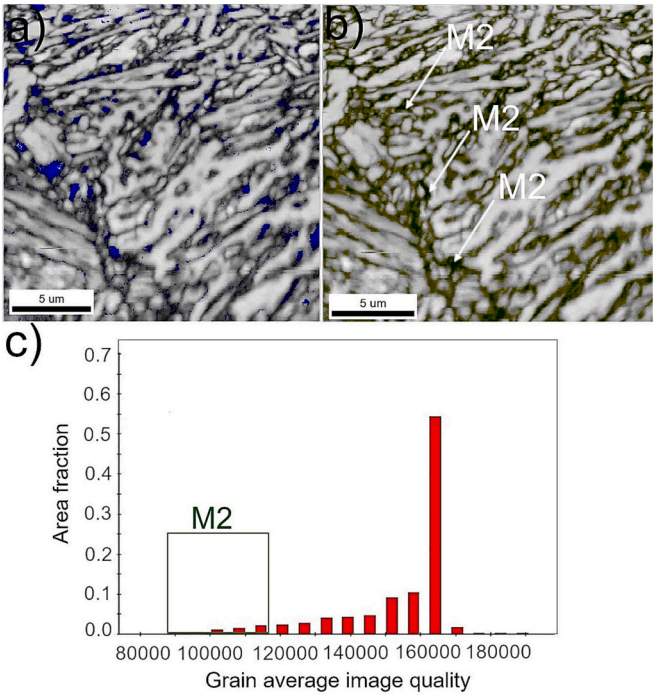

Fig. 14. EBSD maps of investigated steel after second IA step performed at 850 °C for 30s, heated and cooled at rates of 80 °C/s and 60 °C/s, respectively: a) image quality map combined with phase distribution map (RA marked in blue); b) image quality map with selected areas showing the lowest IQ parameter corresponding to the M2-type martensite (marked in green); c) area fraction of the grain average IQ corresponding to the M2-type martensite (marked in green in Fig. 14b). (For interpretation of the references to colour in this figure legend, the reader is referred to the web version of this article).

850 °C, the fraction of austenite was high (Fig. 7) and thus almost all fraction of this phase transformed into martensite during cooling to room temperature. The amount of RA was the smallest (3.1% vol.) for specimens after second IA step performed using heating and cooling rates of 80 °C/s and 60 °C/s, respectively. The XRD method allows to distinguish the volume fraction of BCC and FCC phases. The fractions of austenite (FCC) for particular heat treatment variants are shown in Table 2. Ferrite and martensite are BCC phases; thus it is not possible to distinguish them based on the XRD method. However, taking into account that a ferrite fraction after second IA was very small (Fig. 8a-c), it can be assumed that the remaining volume fraction in Table 2 is martensite. The average fractions of martensite for particular heat treatment variants were listed in Table 2. Obtained results are in good agreement with the dilatometric data (Fig. 2 and Fig. 3) and they are also consistent with the trend of the EBSD measurements (Figs. 9-11). The fractions of RA in specimens after DSIA were relatively small: from 3.1%vol. to 5.1%vol. This is related to the high annealing temperature of 850 °C, at which a high fraction of intercritical austenite was formed. However, the significant fraction of this intercritical austenite was insufficiently enriched in C and Mn and consequently unstable at room temperature. In case of steel produced via one-step IA, the fraction of RA is usually from 20% to 40% [4–7]. However, the aim of the second annealing step is to produce a high fraction of low-C martensite instead of soft ferrite in order to increase strength properties of medium-Mn steels and to reduce the difference in hardness between particular microstructural constituents. It is beneficial to the local deformability of sheet edges [12,13]. The amount of RA obtained in this study is at a similar level to quenching and partitioning (QP) steels with the microstructure composed of low-C martensite and retained austenite [35,41]. The main contribution to mechanical properties in steels produced via the double-step IA and QP heat treatments is due to low-C ductile martensite and the TRIP effect to a lesser extent.

Results obtained by Glover et al. [14] showed that the replacement of ferrite with low-C martensite in the final microstructure improves the strength-ductility product of 0.14C–7.14Mn–0.21Si steel. Moreover, the formation of this low carbon martensite prevents discontinuous yielding of investigated steel due to introduction of a large volume fraction of mobile dislocations. The mechanical properties investigations are a subject of ongoing studies.

4. Conclusions

Effects of different heating and cooling rates on the microstructure of double soaked intercritically annealed Al-alloyed medium-Mn steel was studied in detail by using microscopic techniques of different resolutions. The following conclusions were drawn:

- The proposed heat treatment resulted in the formation of complex microstructures containing a small fraction of ferrite, retained austenite and two types of martensite for all applied heating and cooling rates. Lath martensite less enriched in C/Mn and blocky martensite characterized by higher C/Mn content were identified. RA is located near the martensite more enriched in C/Mn.
- Applied heating rates remarkably affect the kinetics of austenite formation during second IA step. A lower heating rate (3 °C/s) results in more stable austenite due to the longer time for enriching this phase in C and Mn from ferrite, primary austenite and Mn-rich cementite.
- Application of a low heating rate of 3 °C/s in combination with a high cooling rate of 60 °C/s resulted in the highest thermal stability of retained austenite and its highest fraction (5.1 vol%) in the final microstructure. It is related to more homogenous distribution of C/Mn within this phase.

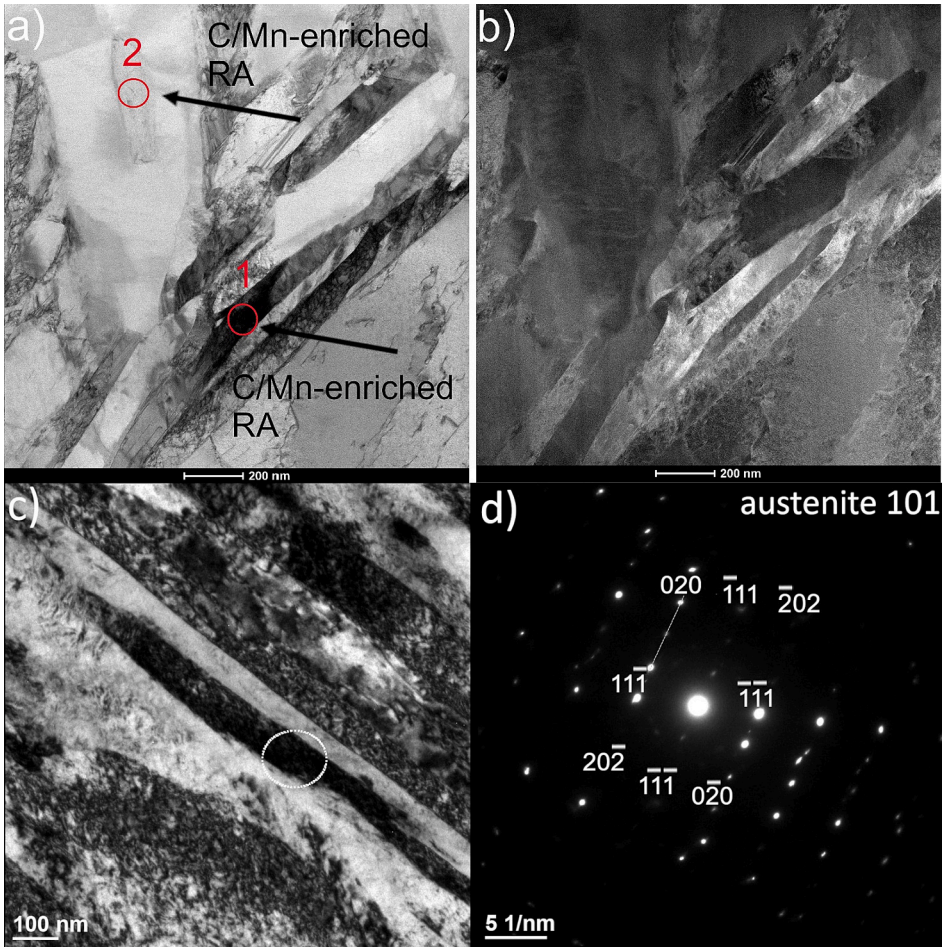

Fig. 15. STEM and TEM images of specimen heated and cooled at rates of 80 °C/s and 60 °C/s: a) STEM bright field image, b) STEM annular dark-field image, c) TEM bright image, d) selected area diffraction pattern of austenite. Points 1 and 2 (red circles): TEM-EDS areas. (For interpretation of the references to colour in this figure legend, the reader is referred to the web version of this article).

Table 2
Fraction of retained austenite and martensite+ferrite (XRD) in investigated samples processed by using different heating and cooling rates.

Specimen Type	Fraction of FCC phase (RA), % vol.	Fraction of BCC phase (maretnsite and ferrite), % vol.
Initial state (after first IA)	19.4 ± 2.3	80.6 ± 2.3
850_80_60	3.1 ± 0.8	96.9 ± 0.8
850_80_10	4.2 ± 0.9	95.8 ± 0.9
850_3_60	5.1 ± 0.9	94.9 ± 0.9

- The applied range of heating and cooling rates have no significant effect on the grain size and morphology of all microstructural constituents.

Declaration of Competing Interest

The authors declare that they have no conflict of interest.

Data availability

The data that support the findings of this study are available from the corresponding author upon reasonable request.

Acknowledgements

Aleksandra Kozłowska acknowledges the scientific internship at Ghent University, Department of Electromechanical, Systems and Metal Engineering, Research Group Materials Science and Technology, Ghent, Belgium in December 2021. The publication was supported under the Initiative of Excellence—Research University program implemented at the Silesian University of Technology in 2020, grant no. 10/010/SDU/10-21-01.

The authors would like to thank MSc Krzysztof Matus for his valuable assistance in transmission electron microscopy (TEM) investigations.

References

[1] D. Raabe, B. Sun, A. Kwiatkowski Da Silva, B. Gault, H.W. Yen, K. Sedighiani, P. H. Sukumar, I.R. Souza Filho, S. Katnagallu, E. Jagle, P. Kurnsteiner, N. Kusampudi, L. Stephenson, M. Herbig, C.H. Liebscher, H. Springer, S. Zaefferer, V. Shah, S.L. Wong, C. Baron, M. Diehl, F. Roters, D. Ponge, Current challenges and opportunities in microstructure-related properties of advanced high-strength steels, Metall. Mater. Trans. A 51 (2020) 5517–5586, https://doi.org/10.1007/s11661-020-05947-2.

[2] F. Czerwinski, Current trends in automotive lightweighting strategies and materials, Materials 663 (2021), https://doi.org/10.3390/ma14216631.

[3] Z. Xu, X. Shen, T. Allam, W. Song, W. Bleck, Austenite reversion and nano-precipitation during a compact two-step heat treatment of medium-Mn steel containing Cu and Ni, J. Mater. Res. Technol. 17 (2022) 2601–2613, https://doi.org/10.1016/j.jmrt.2022.02.008.

[4] G. Liu, B. Li, S. Xu, S. Tong, X. Wang, X. Liang, X. Sun, Effect of intercritical annealing temperature on multiphase microstructure evolution in ultra-low carbon medium manganese steel, Mater. Charact. 173 (2021), 110920, https://doi.org/10.1016/j.matchar.2021.110920.

[5] A.K. Chandan, G.K. Bansal, J. Kundu, J. Chakraborty, S.G. Chowdhury, Effect of prior austenite grain size on the evolution of microstructure and mechanical properties of an intercritically annealed medium manganese steel, Mater. Sci. Eng. A 786 (2019), 138458, https://doi.org/10.1016/j.msea.2019.138458.
[6] R.S. Varanasi, B. Gault, D. Ponge, Effect of Nb micro-alloying on austenite nucleation and growth in a medium manganese steel during intercritical annealing, Acta Mater. 229 (2022), https://doi.org/10.1016/j.actamat.2022.117786.
[7] A. Skowronek, A. Grajcar, A. Kozłowska, A. Janik, M. Morawiec, R.H. Petrov, Temperature-dependent microstructural evolution of Al-rich medium-Mn steel during intercritical annealing, Metall. Mater. Trans. A 53 (2022) 3012–3021, https://doi.org/10.1007/s11661-022-06721-2.
[8] Q. Guo, H.W. Yen, H. Luo, S.P. Ringer, On the mechanism of Mn partitioning during intercritical annealing in medium Mn steels, Acta Mater. 225 (2022), 117601, https://doi.org/10.1016/j.actamat.2021.117601.
[9] R. Kalsar, S. Sanamar, N. Schell, H.G. Brokmeier, R. Saha, R. Ghoshd, A.N. Bhagat, S. Suwas, Elemental partitioning in medium Mn steel during short-time annealing: an in-situ study using synchrotron x-rays, Materialia 9 (2020) 100594, https://doi.org/10.1016/j.mtla.2020.100594.
[10] R.S. Varanasi, S. Zaefferer, B. Sun, D. Ponge, Localized deformation inside the Lüders front of a medium manganese steel, Mater. Sci. Eng. A 824 (2021), 141816, https://doi.org/10.1016/j.msea.2021.141816.
[11] Y.Z. Liang, Z.H. Cao, J. Lu, M.X. Huang, C.C. Tasan, Influence of co-existing medium Mn and dual phase steel microstructures on ductility and Lüders band formation, Acta Mater. 221 (2021), 117418, https://doi.org/10.1016/j.actamat.2021.117418.
[12] N. Pathak, C. Butcher, M. Worswick, Assessment of the critical parameters influencing the edge stretchability of advanced high-strength steel sheet, J. Mater. Eng. Perform. 25 (2016) 4919–4932.
[13] S. Park, J. Jung, W. Cho, B.S. Jeong, H. Na, S.I. Kim, M.G. Lee, N.H. Han, Predictive dual-scale finite element simulation for hole expansion failure of ferrite-bainite steel, Int. J. Plast. 136 (2021), 102900, https://doi.org/10.1016/j.ijplas.2020.102900.
[14] J. Speer, R. Rana, D. Matlock, A. Glover, G. Thomas, E. De Moor, Processing variants in medium-Mn steels, Metals 9 (2019), https://doi.org/10.3390/met907077.
[15] A. Glover, P.J. Gibbs, C. Liu, D.W. Brown, B. Clausen, J.G. Speer, E. De Moor, Deformation behavior of a double soaked medium manganese steel with varied martensite strength, Metals 761 (2019), https://doi.org/10.3390/met9070761.
[16] A. Glover, J.G. Speer, E. De Moor, Tempering and austempering of double soaked medium manganese steels, Front Mater. 7 (2021), 622131, https://doi.org/10.3389/fmats.2020.622131.
[17] K. Steineder, R. Schneider, D. Krizan, C. Béal, C. Sommitsch, Comparative investigation of phase transformation behavior as a function of annealing temperature and cooling rate of two medium-Mn steels, Steel Res. Int. 86 (2015) 1179–1186, https://doi.org/10.1002/srin.201400551.
[18] K. Steineder, D. Krizan, R. Schneider, C. Béal, C. Sommitsch, On the microstructural characteristics influencing the yielding behavior of ultra-fine grained medium-Mn steels, Acta Mater. 139 (2017) 39–50, https://doi.org/10.1016/j.actamat.2017.07.056.
[19] P.J. Gibbs, E. De Moor, M.J. Merwin, B. Clausen, J.G. Speer, D.K. Matlock, Austenite stability effects on tensile behavior of manganese-enriched-austenite transformation-induced plasticity steel, Metall. Mater. Trans. A 42 (2011) 3691–3702, https://doi.org/10.1007/s11661-011-0687-y.
[20] B. Hu, H. Luo, A novel two-step intercritical annealing process to improve mechanical properties of medium Mn steel, Scr. Mater. 176 (2019) 250–263, https://doi.org/10.1016/j.actamat.2019.07.014.
[21] Q. Ye, G. Han, J. Xu, Z. Cao, L. Qiao, Y. Yan, Effect of a two-step annealing process on deformation-induced transformation mechanisms in cold-rolled medium manganese steel, Mater. Sci. Eng. A 831 (2022), 142244, https://doi.org/10.1016/j.msea.2021.142244.
[22] S. Jing, H. Ding, Y. Ren, Z. Cai, A new insight into annealing parameters in tailoring the mechanical properties of a medium Mn steel, Scr. Mater. 202 (2021), 114019, https://doi.org/10.1016/j.scriptamat.2021.114019.
[23] E.I. Hernandez-Duran, T. Ros-Yanez, F.M. Castro-Cerda, R.H. Petrov, The influence of the heating rate on the microstructure and mechanical properties of a peak annealed quenched and partitioned steel, Mater. Sci. Eng. A 797 (2020), 140061, https://doi.org/10.1016/j.msea.2020.140061.
[24] D.P. Yang, D. Wu, H.L. Yi, Comments on "The effects of the heating rate on the reverse transformation mechanism and the phase stability of reverted austenite in medium Mn steels" by J. Han, Y.K. Lee, Acta Mater., 67 (2014), 354-361, Scr. Mater. 147 (2020) 11–13, https://doi.org/10.1016/j.scriptamat.2019.07.040.
[25] B. Hu, X. Shen, Q. Guo, Q. Wen, X. Tu, C. Ding, F. Ding, W. Song, H. Luo, Yielding behaviour of triplex medium Mn steel alternated with cooling strategies altering martensite/ferrite interfacial feature, J. Mater. Sci. Technol. 126 (2022) 60–70, https://doi.org/10.1016/j.jmst.2022.04.003.
[26] J. Han, Y.K. Lee, The effects of the heating rate on the reverse transformation mechanism and the phase stability of reverted austenite in medium Mn steels, Acta Mater. 67 (2014) 354–361, https://doi.org/10.1016/j.actamat.2013.12.038.
[27] Y. Ma, B. Sun, A. Schoekel, W. Song, D. Ponge, D. Raabe, W. Bleck, Phase boundary segregation-induced strengthening and discontinuous yielding in ultrafine-grained duplex medium-Mn steels, Acta Mater. 200 (2020) 389–403, https://doi.org/10.1016/j.actamat.2020.09.007.
[28] P. Wen, B. Hu, J. Han, H. Luo, A strong and ductile medium Mn steel manufactured via ultrafast heating process, J. Mater. Sci. Technol. 97 (2022) 54–68, https://doi.org/10.1016/j.jmst.2021.04.035.
[29] A. Grajcar, A. Skrzypczyk, D. Woźniak, Thermomechanically rolled medium-Mn steels containing retained austenite, Arch. Metall. Mater. 59 (2014) 1691–1697, https://doi.org/10.2478/amm-2014-0286.
[30] ASTM A1033–04, Standard Practice for Quantitative Measurement and Reporting of Hypoeutectoid Carbon and Low-Alloy Steel Phase Transformations; ASTM International: West Conshohocken. https://www.astm.org/, 2018.
[31] J.J. Mueller, X. Hu, X. Sun, Y. Ren, K. Choi, E. Barker, J.G. Speer, D.K. Matlock, E. De Moor, Austenite formation and cementite dissolution during intercritical annealing of a medium-manganese steel from a martensitic condition, Mater. Des. 203 (2021), 109598, https://doi.org/10.1016/j.matdes.2021.109598.
[32] D.T. Han, Y.B. Xu, F. Peng, Y. Zou, R.D.K. Misra, The determining role of pre-annealing on Mn partitioning behavior in medium-Mn-TRIP steel: experimental and numerical simulation, J. Mater. Sci. 55 (2020) 4437–4452, https://doi.org/10.1007/s10853-019-04256-3.
[33] D.P. Yang, D. Wu, H.L. Yi, Reverse transformation from martensite into austenite in a medium-Mn steel, Scr. Mater. 161 (2019) 1–5, https://doi.org/10.1016/j.scriptamat.2018.09.046.
[34] J. Hidalgo, C. Celada-Casero, M.J. Santofimia, Fracture mechanisms and microstructure in a medium Mn quenching and partitioning steel exhibiting macrosegregation, Mater. Sci. Eng. A 754 (2019) 766–777, https://doi.org/10.1016/j.msea.2019.03.055.
[35] D. De Knijf, R. Petrov, C. Föjer, L.A.I. Kestens, Effect of fresh martensite on the stability of retained austenite in quenching and partitioning steel, Mater. Sci. Eng. A 615 (2014) 107–115, https://doi.org/10.1016/j.msea.2014.07.054.
[36] A. Grajcar, A. Kilarski, A. Kozłowska, Microstructure-property relationships in thermomechanically processed medium-Mn steels with high Al content, Metals 8 (2018) 929, https://doi.org/10.3390/met8110929.
[37] A.S. Podder, H.K.D.H. Bhadeshia, Thermal stability of retained austenite in bainitic steels, Mater. Sci. Eng. A 527 (2010) 2121–2128, https://doi.org/10.1016/j.msea.2009.11.063.
[38] E.V. Pereloma, A.A. Gazder, I.B. Timokhina, Addressing retained austenite stability in advanced high strength steels, Mater. Sci. Forum 738 (2012) 212–216.
[39] I. de Diego-Calderón, M.J. Santofimia, J.M. Molina-Aldareguia, M.A. Monclús, I. Sabirov, Deformation behavior of a high strength multiphase steel at macro- and micro-scales, Mater. Sci. Eng. A 611 (2014) 201–211, https://doi.org/10.1016/j.msea.2014.05.068.
[40] Q. Guo, H.W. Yen, H. Luo, S.P. Ringer, On the mechanism of Mn partitioning during intercritical annealing in medium Mn steels, Acta Mater. 225 (2022), 117601, https://doi.org/10.1016/j.actamat.2021.117601.
[41] M.J. Santofimia, L. Zhao, R. Petrov, J. Sietsma, Characterization of the microstructure obtained by the quenching and partitioning process in a low-carbon steel, Mater. Charact. 59 (2008) 1758–1764, https://doi.org/10.1016/j.matchar.2008.04.004.